Properties of proton drip-line nuclei at the *sd*-*fp*-shell interface

W. E. Ormand
Physics Department, 401 Nielsen Hall, University of Tennessee, Knoxville, Tennessee 37996
and Physics Division, Oak Ridge National Laboratory, P.O. Box 2008, MS-6373 Building 6003, Oak Ridge, Tennessee 37831
(Received 7 August 1995)

Properties of proton-rich nuclei at the *sd*-*fp*-shell boundary with $37 \leqslant A \leqslant 48$ are investigated within the framework of the nuclear shell model. Predicted binding energies, one- and two-proton separation energies, and β-end-point energies are presented. Half-lives associated with one- and two-proton emissions are compared with β decay, and it is determined that the best candidates for the observation of correlated two-proton emission are ^{38}Ti and ^{45}Fe. The predicted branching ratios for β decay as a function of excitation energy in the daughter nucleus are shown. Where available, β-decay half-lives are compared with experiment and are found to be in overall good agreement.

PACS number(s): 21.10.Dr, 21.10.Tg, 23.50.+z, 27.40+z

I. INTRODUCTION

With the development of radioactive ion beam facilities, detailed studies of the properties of nuclei along the proton drip line will be possible. This represents a new and exciting development in nuclear structure physics from both experimental and theoretical points of view. By studying the properties of nuclei with a large proton excess, it will be possible to test nuclear-structure models, which have proven to be very successful for nuclei along the valley of stability, at the extremes. An exciting feature of proton-rich nuclei is that new decay modes, such as diproton emission, may be observable. Given that the two-proton system is unbound, it is of particular interest to discover whether diproton emission occurs via the sequential emission of protons through a virtual intermediate state or by the emission of a correlated two-proton system. An important region of study for this phenomenon is the interface between the $0s$-$1d$ (*sd*) and $0f$-$1p$ (*fp*) shells, in particular, those nuclei with active valence protons in the *fp* shell and neutron holes in the *sd* shell.

Diproton emission is a decay process that is allowed because of the odd-even staggering in binding energy. Because of the pairing interaction, the system with an even number of protons (Z,N) is generally more tightly bound than the $(Z-1,N)$ nucleus, but because of the symmetry energy and Coulomb repulsion, it is unbound relative to the $(Z-2,N)$ system. Similar to single-proton emission, the decay rate for diproton emission is determined by the penetrability factor P_C to tunnel through the Coulomb barrier. Because of the higher charge of the two-proton system, however, the Coulomb barrier is higher, and the decay rate for diproton emission is much slower in comparison to proton emission with the same separation energy. In addition, because of the large Coulomb energy difference between (Z,N) and $(Z-1,N+1)$ nuclei, the β-decay end-point energy is quite large, and the corresponding β-decay lifetime is very short ($\sim$10–50 ms). As such, we may expect a competition between β-decay and diproton emission.

The β-decay lifetimes of proton-rich nuclei are short because of two effects caused by the large Q_β value (or β-end-point energy E_β). The first is an obvious effect in that the lifetime is proportional to E_β^{-5}. The second effect is that because of the large Q_β value, the Fermi transition to the analog state is allowed and Gamow-Teller transitions can occur to a large number of states in the final nucleus. Indeed, with an end-point energy of the order of 11–18 MeV, several hundred Gamow-Teller transitions are possible. Because of the phase-space factor, however, those states with the largest β end point tend to dominate the decay.

As is pointed out in Ref. [1], one β decay in the mass region being studied here that deserves special attention is that for ^{40}Ti. The importance of ^{40}Ti is that it is the analog of ^{40}Ar, which is the medium for detecting solar neutrinos with the ICARUS detector. Contrary to the initial ICARUS design assumptions [2], Gamow-Teller transitions were found to be significant, increasing the absorption cross section by a factor of 3 [1]. Fortunately, because of the large Q_β value for ^{40}Ti, all transitions of significance for neutrino absorption on ^{40}Ar are experimentally accessible in the β decay, and a calibration of ICARUS for neutrino detection is possible.

In this paper, a shell-model study of nuclei at the interface of the *sd* and *fp* shells is carried out. Absolute binding energies, and, therefore, one- and two-proton separation energies, are evaluated by adding a computed Coulomb energy shift between analog nuclei to the experimentally measured binding energy of the neutron-rich member. The Coulomb energy shifts were evaluated using an interaction determined empirically by fitting to experimental b and c coefficients [3]. The predicted binding energies are expected to be accurate at the level of 50–150 keV. The β-decay properties of several nuclei, including lifetimes and branching ratios, are presented. Where possible, comparison with experiment is made. Last, the expected lifetimes for β decay and single-proton and diproton emission are compared with an eye towards choosing the best candidate for observing diproton decay.

The paper is organized in the following manner. In Sec. II, the method for computing absolute binding energies is outlined. In Sec. III, the β-decay properties of $^{38-41}$Ti, $^{42-44}$V, $^{42-45}$Cr, ^{46}Mn, and ^{45,46}Fe are presented. Comparisons between particle emission and β-decay lifetimes are given in Sec. IV, and concluding remarks are given in Sec. V.

II. BINDING ENERGIES

Within the framework of the nuclear shell model, accurate absolute binding energies are somewhat difficult to evaluate directly. This is because the dominant part of the nuclear Hamiltonian, which is isoscalar, is usually determined empirically by fitting to experimental binding energies that have had the Coulomb energy subtracted off in an average way (cf. [4,5]). As such, the resulting isoscalar nuclear Hamiltonian may contain residual parts associated with the isoscalar part of the Coulomb interaction.

On the other hand, it is rather straightforward to compute the Coulomb energy shifts within an isobaric multiplet as was demonstrated in Refs. [3,6,7]. The binding energy of the members within a multiplet with A nucleons, isospin T, and z component of the isospin $T_z=(Z-N)/2$ can accurately be reproduced with the isobaric mass multiplet equation (IMME) [8–10]

$$\mathrm{BE}(A,T,T_z,i)=a(A,T,i)+b(A,T,i)T_z+c(A,T,i)T_z^2, \tag{1}$$

where i denotes all other quantum numbers, and the coefficients a, b, and c depend on the isoscalar [12], isovector, and isotensor components of the nuclear Hamiltonian, respectively. In Ref. [3], empirical isovector and isotensor Hamiltonians were obtained for several shell-model spaces. The deviations between theory and experiment varied from space to space, but on average the rms deviations for b and c coefficients were of the order 30 keV and 15 keV, respectively.

From Eq. (1), the binding energy difference between isobaric analogs with $T_z=\pm T$ is given by

$$\mathrm{BE}(A,T,T_z=T,i)-\mathrm{BE}(A,T,T_z=-T,i)=2b(A,T,i)T. \tag{2}$$

Therefore, an accurate way to predict binding energies for proton-rich nuclei is to compute the b coefficient for the multiplet (or analog Coulomb energy difference) and add $2bT$ to the experimental binding energy $\mathrm{BE}_{\mathrm{expt}}(A,T,T_z=-T,i)$ of the neutron-rich member. Here, the experimental binding energies were taken from the 1993 atomic mass tables of Audi and Wapstra [11].

For the nuclei under consideration in this work, the Coulomb energy shifts were evaluated using the shell-model code OXBASH [13] in proton-neutron formalism. The configuration space consisted of the $0d_{3/2}$ and $0f_{7/2}$ orbitals, while the isoscalar Hamiltonian is given in Ref. [14]. The Coulombic, or isospin nonconserving (INC), interaction is described in Ref. [3], and was fit to 22 b and 13 c coefficients using the same base isoscalar interaction. The rms deviation between the fitted and experimental b coefficients was 21.2 keV. The uncertainty in the predicted binding energy for the $T_z=T$ nucleus is therefore (in keV)

$$\delta\mathrm{BE}(A,T,T_z=T,i)$$

$$=\sqrt{(42T)^2-\delta(\mathrm{BE}_{\mathrm{expt}}(A,T,T_z=-T,i))^2}, \tag{3}$$

where $\delta\mathrm{BE}_{\mathrm{expt}}(A,T,T_z=-T,i)$ is the uncertainty in the experimental binding energy.

An important parameter for the INC interaction is the oscillator frequency $\hbar\omega$, as the Coulomb components are scaled as a function of A by the factor [3]

$$S(A)=\left[\frac{\hbar\omega(A)}{11.096}\right]^{1/2}. \tag{4}$$

For the most part, $\hbar\omega$ is chosen to reproduce experimental rms charge radii, and for many nuclei it can be accurately parametrized by

$$\hbar\omega(A)=45A^{-1/3}-25A^{-2/3}\ \mathrm{MeV}. \tag{5}$$

It is important to note, however, that for $A\geqslant 45$, Eq. (5) underestimates $\hbar\omega$ as compared to values derived from experimental charge radii. Indeed, in Ref. [3], the value of 10.222 MeV was used for $A=53$. In addition, a similar INC interaction was recently developed for *fp*-shell nuclei, and better agreement between theoretical and experimental Coulomb energy shifts was obtained with oscillator frequencies derived from the rms charge radii of Hartree-Fock calculations using the Skyrme M^* interaction [15]. In Ref. [3], no nuclei in the mass region $44\leqslant A\leqslant 48$ were included in the fits to the INC interaction, and as such b coefficients for nuclei with $A=45$–46 are significantly underpredicted. To account for the discrepancy between Eq. (5) and experimental values for heavier nuclei, $\hbar\omega$ for $44\leqslant A\leqslant 48$ was fixed so as to reproduce some experimental data. For $A=45$–47, experimental b coefficients obtained between mirror nuclei were used, while for $A=44$ and 48, Coulomb shifts between analog states in Sc and Ca isotopes were used. The values of $\hbar\omega$ used for these nuclei are 10.841, 10.844, 10.886, 10.760, and 10.738 (in MeV) for $A=$ 44, 45, 46, 47, and 48, respectively.

It should be pointed out that Eq. (2) was also used in Ref. [16] to obtain absolute binding energies. For the purely *fp*-shell nuclei (i.e., those nuclei that to first order close the *sd* shell), the b coefficients for Eq. (2) were obtained from a shell-model calculation using only the $0f_{7/2}$ orbit and an INC interaction determined in Ref. [7]. On the other hand, a simplified, ''weak-coupling'' approximation was used for the cross-shell nuclei, and the b coefficients did not depend on the structure of the state. In contrast, a fully microscopic calculation utilizing the same shell-model configuration space for all nuclei under consideration was carried out here. For the most part, the two approaches are in overall agreement, with some differences at the level of 200–300 keV being observed. In addition, due to a global rms deviation between experimental and fitted b coefficients of 21 keV, the uncertainties quoted here are somewhat larger. Last, predictions for some nuclei not included in Ref. [16] are reported here.

Shown in Table I are the results obtained for proton-rich nuclei whose binding energies are unknown in the mass region $37\leqslant A\leqslant 48$. The table lists the experimental binding energy of the neutron-rich analog, the predicted binding energy, and one- and two-proton separation energies, as well as the β-decay end-point energy.

One nucleus listed in Table I deserves special consideration. This is ^{47}Ni, which, to first order, has eight protons in the *fp* shell and a single neutron hole in the *sd* shell. One can

TABLE I. Predicted binding energies, one- and two-proton separation energies (S_p and S_{2p}, respectively), and β-decay end-point energies for proton-rich nuclei with $37 \leqslant A \leqslant 48$. The absolute binding energies were computed with theoretical Coulomb energy shifts added onto the experimental binding energy for the neutron-rich analog, also listed in the table.

^{A}Z	T_z	J^π	BE_{theor} (MeV)	^{A}Z analog	BE_{expt} analog [a] (MeV)	S_p (MeV)	S_{2p} (MeV)	E_β (MeV)
^{37}Sc	5/2	$7/2^-$	278.490(105)	^{37}S	313.017	-2.870(112)	-0.309(107)	-
^{38}Sc	2	2^-	295.008(84)	^{38}Cl	323.208	-1.144(86)	2.358(84)	-
^{38}Ti	3	0^+	278.928(126)	^{38}S	321.054(7)	0.438(164)	-2.432(132)	15.298(151)
^{39}Sc	3/2	$7/2^-$	312.483(63)	^{39}Ar	333.941(5)	-0.639(63)	3.910(63)	-
^{39}Ti	5/2	$3/2^+$	295.486(105)	^{39}Cl	331.281(2)	0.478(134)	-0.666(107)	16.215(122)
^{39}V	7/2	$7/2^-$	275.470(155)	^{39}S	325.430(50)	-3.458(193)	-3.020(180)	-
^{40}Ti	2	0^+	314.727(84)	^{40}Ar	343.810	2.244(105)	1.605(84)	11.441(85)
^{40}V	3	2^-	293.455(130)	^{40}Cl	337.110(30)	-2.031(164)	-1.553(151)	-
^{40}Cr	4	0^+	275.087(284)	^{40}S	333.180(230)	-0.383(223)	-3.841(210)	17.586(312)
^{41}Ti	3/2	$3/2^+$	329.404(63)	^{41}K	351.618	2.454(63)	2.993(63)	12.951(63)
^{41}V	5/2	$7/2^-$	312.993(159)	^{41}Ar	349.909	-1.734(149)	-0.510(122)	-
^{41}Cr	7/2	$3/2^+$	293.198(103)	^{41}Cl	344.960(60)	-0.257(196)	-2.288(180)	19.013(180)
^{42}V	2	2^-	329.092(84)	^{42}K	359.152	-0.312(105)	2.142(84)	17.031(84)
^{42}Cr	3	0^+	314.275(132)	^{42}Ar	359.340(40)	1.282(203)	-0.452(151)	14.035(151)
^{43}V	3/2	$7/2^-$	346.994(63)	^{43}Ca	369.828	0.089(63)	3.857(63)	11.368(63)
^{43}Cr	5/2	$3/2^+$	330.540(105)	^{43}K	368.795(9)	1.448(134)	1.136(122)	15.650(122)
^{43}Mn	7/2	$7/2^-$	311.512(163)	^{43}Ar	364.960(70)	-2.763(210)	-1.481(228)	-
^{44}V	1	2^+	360.952(42)	^{44}Sc	376.524(2)	1.777(43)	6.265(42)	13.740(42)
^{44}Cr	2	0^+	349.816(84)	^{44}Ca	380.960(1)	2.822(105)	2.911(84)	10.354(94)
^{44}Mn	3	2^-	329.271(132)	^{44}K	376.080(40)	-1.269(164)	0.179(151)	-
^{44}Fe	4	0^+	310.911(169)	^{44}Ar	373.318(20)	-0.601(234)	-3.364(210)	17.578(211)
^{45}Cr	3/2	$7/2^-$	364.030(63)	^{45}Sc	387.850(1)	3.078(76)	4.855(63)	12.277(65)
^{45}Mn	5/2	$7/2^-$	348.736(105)	^{45}Ca	384.953(10)	-1.080(134)	1.742(122)	-
^{45}Fe	7/2	$3/2^+$	329.261(84)	^{45}K	384.953(10)	-0.010(198)	-1.279(181)	18.693(180)
^{45}Co	9/2	$7/2^-$	307.108(198)	^{45}Ar	378.850(60)	-3.803(260)	-4.404(256)	-
^{46}Mn	2	4^+	364.160(84)	^{46}Sc	396.610(1)	0.076(105)	3.208(94)	17.033(86)
^{46}Fe	3	0^+	350.152(126)	^{46}Ca	398.769(2)	1.416(164)	0.336(151)	13.226(151)
^{46}Co	4	2^-	326.746(169)	^{46}K	391.835(16)	-2.515(224)	-2.525(211)	-
^{46}Ni	5	0^+	305.476(213)	^{46}Ar	386.920(40)	-1.632(291)	-5.435(271)	-
^{47}Mn	3/2	$5/2^-$	382.407(63)	^{47}Ti	407.072(1)	0.432(66)	5.318(66)	11.939(64)
^{47}Fe	5/2	$7/2^-$	366.132(105)	^{47}Sc	407.254(2)	1.972(134)	2.102(122)	15.493(122)
^{47}Co	7/2	$7/2^-$	348.513(147)	^{47}Ca	406.045(2)	-1.639(194)	-0.233(180)	-
^{47}Ni [b]	9/2	$1/2^+$	325.950(289)	^{47}K	400.184(8)	-0.796(353)	-3.311(340)	-
^{48}Mn	1	4^+	397.157(42)	^{48}V	413.904(3)	2.029(44)	6.796(42)	13.523(43)
^{48}Fe	2	0^+	385.191(84)	^{48}Ti	418.699(1)	2.784(105)	3.216(86)	11.184(94)
^{48}Co	3	6^+	365.233(126)	^{48}Sc	415.487(5)	-0.899(164)	1.073(126)	-
^{48}Ni	4	0^+	349.015(168)	^{48}Ca	415.991(4)	0.502(223)	-1.137(210)	15.436(210)

[a] From Ref. [11]. Only uncertainties greater than 1 keV are tabulated.
[b] See text for discussion of ^{47}Ni ground-state properties.

deduce the ground-state spin to be $J^\pi = 1/2^+$ from the analog nucleus ^{47}K. This is counter to the natural expectation of a $3/2^+$ ground state, as is the case for ^{45}K, and seems to also be the assumption used in Ref. [16]. Of course this indicates that at some level the $1s_{1/2}$ orbit is becoming important. Indeed, a $1\hbar\omega$ shell-model calculation using the *sd-fp* shells and the interaction of Ref. [5], which is used extensively in the next section, predicts that the $1/2^+$ and $3/2^+$ states are almost degenerate. In addition, the states are more than 50% single hole in character. Currently, no Coulomb interaction has been developed that includes this extended model space, and the predicted binding energy for ^{47}Ni is obtained by computing the Coulomb energy shift for the $3/2^+$ state, and assuming that the shift for the $1/2^+$ state is the same. The total uncertainty is then increased by the conservative amount of 100 keV in order to account for a possible variation in the Coulomb shifts for these two states.

Shown in Table II are the two-proton separation energies obtained in comparison with those of Ref. [16] for those nuclei that are both proton stable and unbound to diproton

TABLE II. Comparison between the two-proton separation energies S_{2p} of this work and Ref. [12].

^{A}Z	S_{2p} (MeV) This work	S_{2p} (MeV) Ref. [12]
^{38}Ti	-2.432(132)	-
^{39}Ti	-0.666(107)	-0.657(20)
^{42}Cr	-0.452(151)	-0.498(66)
^{45}Fe	-1.279(181)	-1.154(94)
^{48}Ni	-1.137(210)	-1.357(130)

emission. The two methods are in excellent agreement for ^{39}Ti and ^{42}Cr, while for ^{45}Fe and ^{48}Ni, the two results differ by approximately 200 keV, but are in overall agreement because of the larger uncertainties quoted here. Although these differences are not that large, they can have important consequences regarding the expected diproton decay half-life because of the extreme sensitivity to the two-proton separation energy, as will be seen in Sec. IV. Indeed, for this energy region, a 100 keV change in the separation energy can lead to a three-order-of-magnitude change in the half-life. Note the addition of ^{38}Ti to Table II, which was not included in Ref. [16]. In addition to the five candidates listed in Table II, also note two other nuclei in Table I that are predicted to be proton unstable by approximately 200–300 keV, but are unbound to diproton emission by more than 2 MeV. These cases are ^{40}Cr and ^{41}Cr. Because of the large two-proton separation energies, the dominant decay mode for these nuclei may be diproton emission with a very short lifetime (see Sec. IV).

Finally, as an additional check, the Coulomb energy shifts for the purely *fp*-shell nuclei were also computed using the INC interaction of Ref. [15] in conjunction with the FPD6 interaction of Ref. [17] in the *fp* shell, and were found to agree with the values used in Table I to within 50 keV.

III. β-DECAY PROPERTIES

In this section, the β-decay properties of several nuclei listed in Table I are presented. In particular, the half-lives and the distribution of the β-decay strength in the daughter nucleus are shown.

The partial half-life for the β decay from the parent ground state to the ith state in daughter nucleus is given by

$$t_{1/2}^{i}=\frac{K}{G_V^2|\mathscr{M}_{o\to i}|^2 f_{o\to i}}, \tag{6}$$

where $K=2\pi^3(\ln 2)\hbar^7/(m_e^5c^4)$ and $K/G_V^2=6170\pm 4$ s [18]. The square of the transition matrix element $|\mathscr{M}_{o\to i}|^2$ is written as

$$|\mathscr{M}_{o\to i}|^2=[B(F)_{o\to i}+B(\mathrm{GT})_{o\to i}], \tag{7}$$

where, in the long-wavelength limit, the Fermi and Gamow-Teller reduced transition probabilities are given by

$$B(F)_{o\to i}=\frac{1}{2J_o+1}|\langle J_i||t_\pm||J_o\rangle|^2 =[T_o(T_i+1)-T_{zo}T_{zi}]\delta_{o,i}, \tag{8}$$

and

$$B(\mathrm{GT})_{o\to i}=\frac{1}{2J_o+1}\left(\frac{g_A}{g_V}\right)^2|\langle J_i||(\vec{\sigma}t_\pm)_{\mathrm{eff}}||J_o\rangle|^2, \tag{9}$$

with the quantity $g_A/g_V=1.2606\pm 0.0075$ [19] being the ratio of the axial and vector weak-coupling constants. Note that the Fermi transition only occurs between the isobaric analog states (IAS's). Last, in keeping with the observation that experimental B(GT) values are generally quenched relative to theoretical estimates, the free-nucleon Gamow-Teller operators were renormalized by the factor 0.775 [20].

For the statistical rate function $f_{o\to i}$, the formalism of Ref. [21] was used, which is expected to be accurate to within 0.5%, namely,

$$f_{o\to i}=(1+\delta_R+\delta_\beta^{Z\alpha^2}+\delta_\beta^{Z^2\alpha^3})\int_1^{W_0} dW p W(W_0-W)^2 F_0(Z,W)L_0(Z,W)C(Z,W)R(W), \tag{10}$$

where p and W are the electron momentum and energy, respectively, in units of m_ec^2, W_0 being the end point, and $F_0(Z,W)$, $L_0(Z,W)$, $C(Z,W)$, and $R(W)$ are parametrized correction factors given in Ref. [21]. The radiative correction factor δ_R is computed by [22]

$$\delta_R=\frac{\alpha}{2\pi}\frac{\int dW p W(W_0-W)^2 g(W,W_0)}{\int dW p W(W_0-W)^2}, \tag{11}$$

where $g(W,W_0)$ is given by Eq. (III-21) in Ref. [22]. The higher-order radiative corrections are parametrized according to $\delta_\beta^{Z\alpha^2}=4.0\times 10^{-4}|Z|$ and $\delta_\beta^{Z^2\alpha^3}=3.6\times 10^{-6}Z^2$ [21].

The total β-decay half-life is then given by the sum of the individual decay rates, i.e.,

$$\frac{1}{t_{1/2}}=\sum_i \frac{1}{t_{1/2}^i}, \tag{12}$$

while the branching ratio of the decay to the ith state is given by

$$\mathrm{BR}_i=\frac{t_{1/2}}{t_{1/2}^i}. \tag{13}$$

TABLE III. β-decay half-lives for selected nuclei compared with experiment where possible.

^{A}Z	$t_{1/2}^{\text{theor}}$ (ms)	$t_{1/2}^{\text{expt}}$ (ms)
^{38}Ti	22	-
^{39}Ti	29	26^{+8}_{-7} (Ref. [23])
^{40}Ti	56	56^{+18}_{-12} (Ref. [23])
^{41}Ti	97	80(2) (Ref. [24])
^{42}V	27	
^{43}V	84	
^{44}V	114	
^{42}Cr	17	
^{43}Cr	14	
^{44}Cr	51	
^{45}Cr	69	
^{46}Mn	37	
^{45}Fe	7	
^{46}Fe	18	
^{48}Ni	9 (Ref. [16])	

Here, the β-decay properties of several nuclei that are expected to be bound to single-proton emission to within 300 keV are computed in the mass region $37 \leqslant A \leqslant 46$. Two classes of nuclei are considered. The first consists of cross *sd-fp*-shell nuclei with valence protons in the *fp* shell, and neutron holes in the *sd* shell, in particular, $^{38-41}$Ti, ^{42}V, ^{42}Cr, ^{43}Cr, and ^{45}Fe. The second class is nuclei whose valence nucleons are in the *fp* shell only, and are ^{43,44}V, ^{44,45}Cr, ^{46}Mn, and ^{46}Fe. For all nuclei, the wave functions were computed in isospin formalism using the shell-model program OXBASH [13]. For the cross-shell nuclei, the *sd-fp* shell valence space combined with the interaction of Ref. [5] was used. The model space for each nucleus was limited to the minimal $\hbar\omega$ excitation to construct the states of the desired parity and isospin as is described in Ref. [5]. Within this context, all possible shell-model configurations were included in the calculations with the exception of ^{45}Fe, where no more than three particles were allowed outside the $0f_{7/2}$ orbit. This restriction was imposed so that the largest dimension for any J,T space was of the order 16 000. For the pure *fp*-shell nuclei, the calculations were carried using the FPD6 interaction of Ref. [17] with no restrictions.

Shown in Table III are the computed β-decay half-lives for each nucleus, and, where possible, a comparison with experimental data is made [23,24]. In addition, for completeness in this mass region, the β-decay half-life of ^{48}Ni given in Ref. [16] is also presented. Because of the strong dependence in the partial half-lives on the end-point energy, the excitation energies in the daughter nuclei were fixed by examining the spectra in the analog, neutron-rich nucleus whenever possible. For the most part, this amounted to fixing the starting point of a particular J^{π},T band in the daughter nucleus. The uncertainty in the theoretical predictions is expected to be at the level of (10–20)%. With approximately 10% being due to the uncertainty in the β end point for each transition, and another (5–10)% due to uncertainties in the theoretical B(GT) values. For the most part, the predicted β-decay half-lives for Ti isotopes are in overall agreement with experiment.

In addition to the transitions listed in Table III, both ^{40}Cr and ^{41}Cr are nearly stable to proton breakup, but were not included because rather severe truncations on the shell-model space would be required in order to render the calculations tractable. As such, the Gamow-Teller matrix elements may be unreliable. Making comparisons with similar cases in Table III, the partial half-lives for β decay can be expected to be of the order 2–10 ms. In addition, these two nuclei are unbound to two-proton emission by more than 2 MeV, and, as will be seen in the next section, their partial half-lives for diproton emission will be shorter by several orders of magnitude. Hence, the dominant decay mode for these two nuclei will most likely be diproton emission with an extremely short lifetime.

In Fig. 1, the branching ratio for each decay is plotted as a function of excitation energy in the daughter nucleus. Generally, the decays are fragmented over a large number of states. However, because of the phase-space factor f of Eq. (10), the distribution is generally weighted toward states with the largest β end point (lowest excitation energy). The exception to this trend is of course the Fermi transition, which occurs to the analog state at higher excitation energy. Even though the β-end-point energy for this state is much smaller than for the low-lying Gamow-Teller transitions, the Fermi transition is a competitive decay mode because of the much larger transition amplitude $B(F)$, as can be seen from Eq. (8). Last, note that in essentially all cases, the β decay occurs to final states in the daughter nucleus that are proton unbound.

This section is concluded by noting that isospin-mixing effects have been ignored. At first this may seem to be a bad approximation since the analog state has a high excitation energy in the daughter, and can in principle mix with many background states with isospin $T-1$. As is pointed out in Ref. [1], however, the total Fermi strength is still observable, and the effect of isospin mixing would be to spread the Fermi strength out over a narrow energy window of approximately 100–200 keV because of the rather weak mixing matrix elements. Indeed, it is shown in Ref. [1] the effects of isospin mixing on the total β-decay half-life cancel to first order, leading to uncertainties if the order of 0.2% in the total half-life.

IV. PARTICLE DECAY LIFETIMES

In this section, the partial half-lives for particle emission are examined, and compared with the β-decay half-lives of the previous section. Here, the particle-decay lifetimes are estimated using standard approximations [25–27] namely, that the decay rate, Γ, is given by

$$\Gamma = 2\,\theta^2 \gamma^2 P_L(S), \tag{14}$$

where θ is the shell-model spectroscopic factor, γ^2 is the Wigner reduced width, and $P_L(S)$ is the penetrability factor dependent on both the orbital angular momentum L and the separation energy S. For single-proton emission the reduced width and penetrability factors were evaluated using the WKB approximation as described in Ref. [27], i.e., using Eqs. (12)–(22). For all the proton-rich nuclei under consideration here, the emitted proton has $L=3$. For diproton emission, the penetrabilities and reduced widths were evaluated,

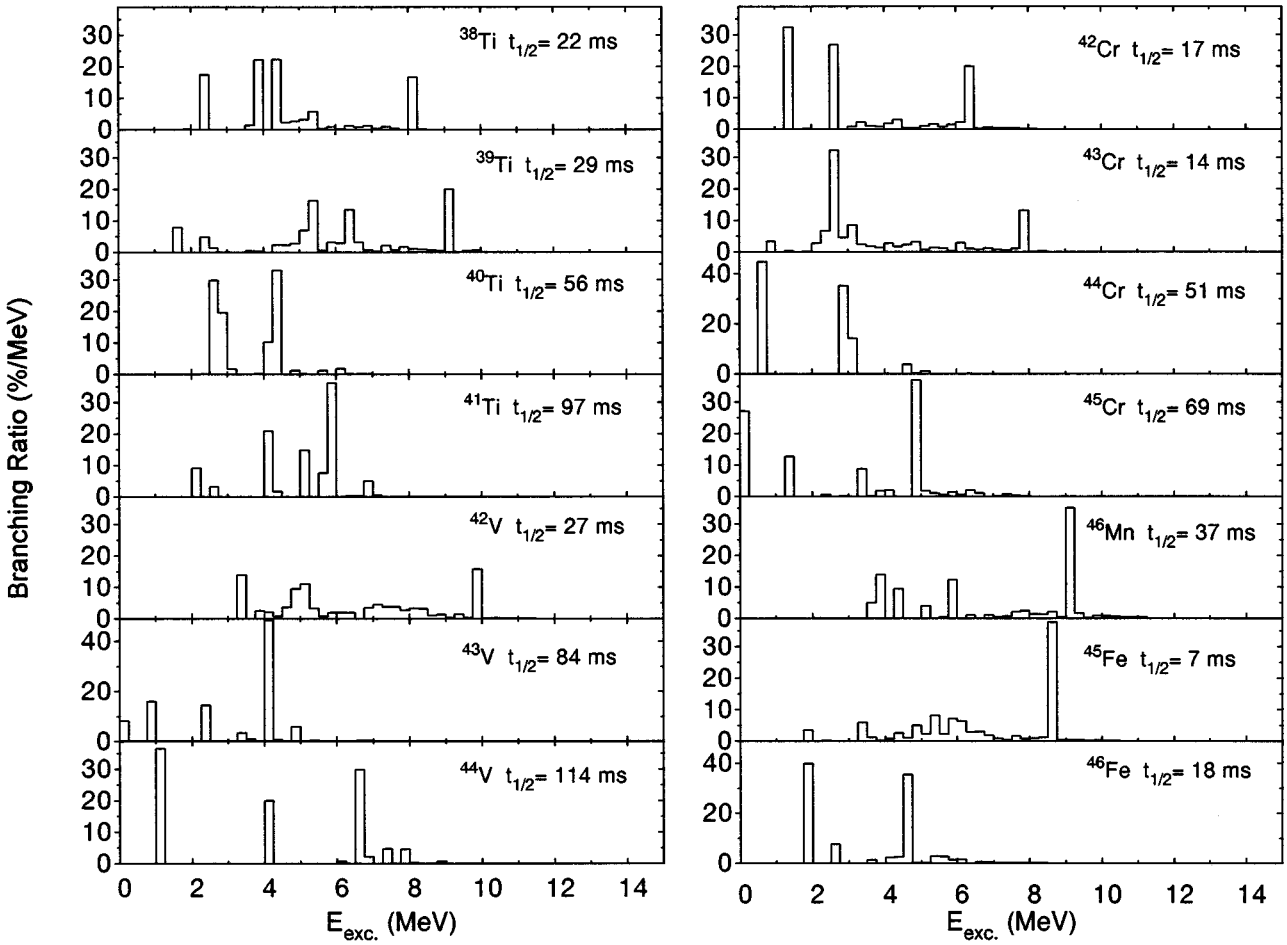

FIG. 1. Plot of the branching ratios as a function of excitation energy in the daughter nucleus for the β decay of $^{38-41}$Ti, $^{42-44}$V, $^{42-45}$Cr, ^{46}Mn, and ^{45,46}Fe. The branching ratios are summed in bins of 250 keV.

as in Ref. [16], using *r*-matrix theory as described in Ref. [25] [in particular Eq. (4.4b)]. The Coulomb wave functions used to compute the penetrabilities were evaluated using Steed's method with an algorithm due to Barnett [28]. Because of the absence of a centrifugal barrier in the $L=0$ channel, the dominant decay mode is expected to occur when the two protons are emitted in a correlated $L=0$ state [29]. The Wigner reduced width is given by

$$\gamma^2 = 3\hbar^2 c^2 / 2\mu R_0^2, \tag{15}$$

where μ is the reduced mass, and the channel radius R_0 was taken to be 4.0 fm. It is to be noted that by decreasing the channel radius to 3.5 fm, the decay rate increases by approximately a factor of 2.

The spectroscopic factor θ can be evaluated within the framework of the shell model. For the emission of a single proton from a single-particle orbit with quantum numbers nlj, the spectroscopic factor is [30]

$$\theta = \frac{1}{\sqrt{2J+1}} \langle \Psi_f(J) || a^\dagger_{nlj} || \Psi_i(J') \rangle. \tag{16}$$

For diproton emission θ^2 can be estimated using cluster-overlap approximation [31], namely,

$$\theta^2 = G^2 [A/(A-k)]^\lambda |\langle \Psi_f | \psi_c | \Psi_i \rangle|^2, \tag{17}$$

where k, λ, and G^2 are parameters dependent on the model space and the emitted cluster, and ψ_c is a two-proton cluster wave function in which the relative motion of the particles is governed by the $0S$ state, and is obtained by diagonalizing an SU(3)-conserving interaction within the shell-model configuration space [31]. For the most part, the spectroscopic factors are generally of the order 0.5–0.75, as is observed in Ref. [16].

On the other hand, the penetrability factor P_L is extremely sensitive to the separation energy. Indeed, for separation energies of the order of 500 keV, an uncertainty of ± 100 keV leads to a range of nearly six orders of magnitude in the half-life. Given that the theoretical uncertainties for each of the diproton emitters are all 100 keV or more, an accurate estimate of the spectroscopic factor is not needed in order to get a reasonable estimate of the diproton lifetime for the purpose of designing experiments. Hence, the lifetimes reported here are evaluated assuming $\theta^2 = 1$, with the understanding that they may be too short by a factor of 2–4 (this also includes uncertainties associated with the channel radius).

To illustrate the sensitivity in the half-life on the separation energy, shown in Fig. 2 are the half-lives associated with

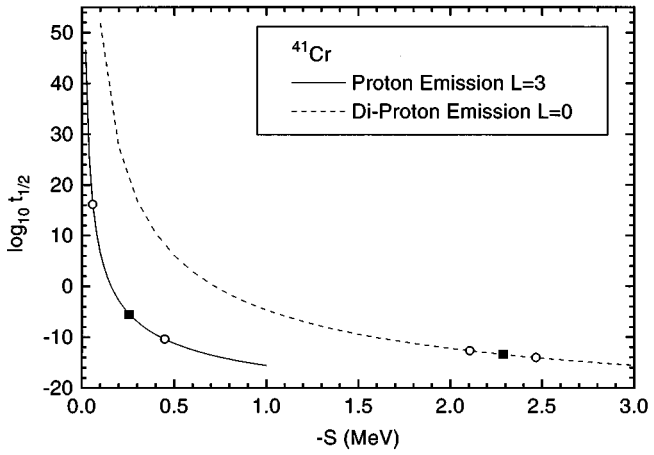

FIG. 2. Logarithmic plot of the half-lives (in seconds) associated with the single-proton and diproton decay of ^{41}Cr as a function of the separation energies S_p and S_{2p}, respectively (note that in the figure $-S$ is plotted). The solid squares represent the half-lives obtained with the separation energies listed in Table I, while the open circles show the range due to the theoretical uncertainty in the separation energies.

^{41}Cr for both single-proton (solid line) and diproton (dashed line) emission as a function of the separation energies S_p and S_{2p} (note that $-S$ is plotted). The solid squares represent the half-lives obtained with the separation energies given in Table I, while the open circles delineate the limits due to the theoretical uncertainties. As can be seen in the figure, because of the uncertainty in the proton separation energy, there is a range in the expected half-life of approximately 16 orders of magnitude. It is also seen that, in order for β decay to be competitive with proton emission in this mass region, the parent nucleus must be unbound by less than 200 keV, which corresponds to a partial half-life of approximately 2–8 ms. From Table I, it is apparent that both ^{45}Fe and ^{46}Mn qualify within this range, while ^{40}Cr, ^{41}Cr, and ^{42}V are at the limits. As in the case for proton decay, diproton emission is also quite sensitive to the separation energy, especially in the region of 0.3–1.0 MeV. Notice from Table III that the β-decay half-lives for all nuclei that are unbound to diproton emission are of the order 10–30 ms. Hence, as can be seen in Fig. 2, the parent nucleus must have a two-proton separation energy less than -1.0 MeV in order for diproton emission to be experimentally observable.

Listed in Table IV are the half-lives associated with diproton emission for $^{38-39}$Ti, ^{42}Cr, ^{45}Fe, and ^{48}Ni. The three values tabulated correspond to the separation energies given in Table I, as well as the minimum and maximum values due to the theoretical uncertainty. In addition, the β-decay half-lives for each case are also shown. Finally, for the purpose of comparison, the range of half-lives for these nuclei obtained in Ref. [16] are also listed.

TABLE IV. Half-lives for diproton emitters compared with β-decay half-lives and the results of Ref. [16].

^{A}Z	$t_{1/2}$ (ms)	$t_{1/2}^{\text{min-max}}$ (ms)	$t_{1/2}^{\beta}$ (ms)	$t_{1/2}^{\text{Ref. [16]}}$ (ms)
^{38}Ti	9×10^{-12}	$(0.4–2.3)\times10^{-12}$	22	-
^{39}Ti	40	0.4–2000	29	28–140
^{42}Cr	10^{11}	10^{5}–10^{19}	17	10^{7}–10^{12}
^{45}Fe	1×10^{-3}	10^{-5}–10^{-1}	7	0.003–0.4
^{48}Ni	3	0.01–3660	9	0.001–0.2

From Table IV, it is seen that the two definitive cases for diproton emission are ^{38}Ti and ^{45}Fe. For both of these nuclei, the partial half-lives for particle emission are several orders of magnitude shorter (even at the extreme upper ranges) than for β decay. Of the two, ^{45}Fe is perhaps the more amenable to experiment since the half-life is expected to be of the order of 1 μs. On the other hand, both ^{39}Ti and ^{48}Ni are marginal cases in that the half-life for diproton emission predicted by the separation energy is expected to be very close to that for β decay. As such, when considering the large range in the half-life associated with the uncertainty in S_{2p}, these lifetimes could be much longer than the β-decay lifetime, and, hence, would not be observable. This conclusion is essentially borne out experimentally for ^{39}Ti, where no evidence of diproton emission was found [23].

Finally, it is noted that an additional feature of ^{45}Fe is that since it has a nonzero ground-state spin, it may be possible to examine the angular correlations of the emitted protons to determine whether the decay occurred via correlated emission or by the emission of two sequential protons. In the latter case, the two protons should be uncorrelated and exhibit the characteristics of particles emitted from an $L=3$ single-particle state.

V. CONCLUSIONS

In this paper, proton-rich nuclei at the interface of the $1s0d$ and $0f1p$ shells are studied in detail. Absolute binding energies were evaluated by computing the Coulomb energy shifts between mirror nuclei, and adding this shift to the experimentally determined binding energy of the neutron-rich isotope. The principal improvement obtained here over previous works, namely, Ref. [16], is in the coherent shell-model treatment of all nuclei in the study. In particular, the Coulomb energy shifts were computed using the same shell-model space and interaction for both the ''purely'' *fp*-shell and the cross-shell nuclei. With the computed binding energies, one- and two-proton separation energies were computed with an eye towards identifying candidates for the experimental observation of diproton emission. Half-lives associated with β decay and diproton emission are presented, and it is concluded that the best candidates for the observation of diproton emission are ^{38}Ti and ^{45}Fe.

ACKNOWLEDGMENTS

Discussions with B. A. Brown, W. Nazarewicz, and B. Zimmermann are gratefully acknowledged. Theoretical nuclear physics research at the University of Tennessee is supported by the U.S. Department of Energy through Contract No. DE-FG05-93ER40770. Oak Ridge National Laboratory is managed for the U.S. Department of Energy by Lockheed Martin Energy Systems, Inc. under Contract No. DE-AC05-84OR21400.

[1] W. E. Ormand, P. M. Pizzochero, P. F. Bortignon, and R. A. Broglia, Phys. Lett. B **345**, 343 (1995).
[2] J. N. Bachall, M. Baldo-Ceolin, C. B. Cline, and C. Rubbia, Phys. Lett. B **178**, 324 (1986).
[3] W. E. Ormand and B. A. Brown, Nucl. Phys. **A491**, 1 (1989).
[4] B. H. Wildenthal, in *Progress in Particle and Nuclear Physics*, edited by D. H. Wilkinson (Pergamon, Oxford, 1984), Vol. 11, p. 5.
[5] E. K. Warburton, J. A. Becker, and B. A. Brown, Phys. Rev. C **41**, 1147 (1990).
[6] R. Sherr and I. Talmi, Phys. Lett. **56B**, 212 (1975); R. Sherr, Phys. Rev. C **16**, 957 (1978); R. D. Lawson, *ibid.* **19**, 2359 (1979); R. R. Whitehead, A. Watt, D. Kelvin, and H. J. Rutherford, Phys. Lett. **65B**, 323 (1976).
[7] B. A. Brown and R. Sherr, Nucl. Phys. **A322**, 61 (1979).
[8] E. P. Wigner, in *Proceedings of the Robert A. Welsch Conference on Chemical Research*, edited by W. O. Milligan (R. A. Welsch Foundation, Houston, Texas, 1958), Vol. 1, p. 88.
[9] W. Benenson and E. Kashy, Rev. Mod. Phys. **51**, 527 (1979).
[10] Assuming only two-body interactions, the IMME is exact at the level of first-order perturbation theory. At present, the only known exception to the IMME is the $J^{\pi}=3/2^{-}, T=3/2$ multiplet for $A=9$ [9].
[11] G. Audi and A. H. Wapstra, Nucl. Phys. **A565**, 1 (1993).
[12] Strictly speaking, the a coefficient contains a small component of the isotensor interaction. See Eq. (2.5a) in Ref. [5].
[13] B. A. Brown, A. Etchegoyen, and W. D. M. Rae, computer code OXBASH, the Oxford University-Buenos Aires-MSU shell model code, Michigan State University Cyclotron Laboratory Report No. 524, 1985.
[14] S. T. Hseih, X. Ji, R. B. M. Mooy, and B. H. Wildenthal, in *Nuclear Structure at High Spin, Excitation and Momentum Transfer*, edited by H. Nann, AIP Conf. Proc. No. 142 (AIP, New York, 1986) p. 356; Bull. Am. Phys. Soc. **30**, 730 (1985).
[15] W. E. Ormand and B. A. Brown, Phys. Rev. C (to be published).
[16] B. A. Brown, Phys. Rev. C **43**, R1513 (1991).
[17] W. A. Richter, M. G. van der Merwe, R. E. Julies, and B. A. Brown, Nucl. Phys. **A523**, 325 (1990).
[18] D. H. Wilkinson, A. Gallman, and D. E. Alburger, Phys. Rev. C **18**, 401 (1978).
[19] D. H. Wilkinson, Nucl. Phys. **A377**, 474 (1982).
[20] B. A. Brown and B. H. Wildenthal, At. Data Nucl. Data Tables **33**, 347 (1985).
[21] D. H. Wilkinson, *Ions lourds et mesons en physique nucleaire/ Nuclear Physics with heavy ions and mesons*, Les Houches, Session XXX (1977), edited by R. Balain *et al.* (North-Holland, Amsterdam, 1978), p. 877.
[22] R. J. Blin-Stoyle, *Fundamental Interactions and the Nucleus* (North-Holland, Amsterdam, 1973).
[23] C. Detraz *et al.*, Nucl. Phys. **A519**, 529 (1990).
[24] R. G. Sextro, R. A. Gough, and J. Cerny, Nucl. Phys. **A234**, 103 (1974).
[25] A. M. Lane and R. G. Thomas, Rev. Mod. Phys. **30**, 257 (1958).
[26] M. H. Macfarlane and J. B. French, Rev. Mod. Phys. **32**, 567 (1960).
[27] S. Hofmann, in *Particle Emission from Nuclei, Vol. II*, edited by D. N. Poenaru and M. S. Evasçu (CRC Press, Boca Raton, FL, 1989), p. 25; S. Hofmann (unpublished).
[28] A. R. Barnett, Comput. Phys. Commun. **27**, 147 (1982).
[29] V. I. Gol'danskii, Nucl. Phys. **19**, 482 (1960); J. Janecke, *ibid.* **61**, 326 (1965).
[30] P. J. Brussaard and P. W. M. Glaudemans, *Shell-Model Applications in Nuclear Spectroscopy* (North-Holland, Amsterdam, 1977).
[31] W. Chung, J. van Hienen, B. H. Wildenthal, and C. L. Bennett, Phys. Lett. **79B**, 381 (1978); J. B. McGrory, *ibid.* **47B**, 481 (1973); M. Ichimura, A. Arima, E. C. Halbert, and T. Terasawa, Nucl. Phys. **A204**, 225 (1973).